AN ARC CODE TO PREDICT THE THERMAL CRACK OF WELDED SAMPLE

Je-Ee Ho

Department of Mechanical and Electrical Engineering, National Ilan University, Ilan, Taiwan, R.O.C., jeho@niu.edu.tw

AN ARC CODE TO PREDICT THE THERMAL CRACK OF WELDED SAMPLE

Je-Ee Ho

ABSTRACT

In this study, a numerical code with enthalpy method in upwind scheme is proposed to estimate the distribution of thermal stress in the molten pool, which is primarily determined by the type of the input power and travel speed of heating source. To predict the cracker deficit inside the workpiece, a simulated program satisfying the diagonal domination and Scarborough criterion provides a stable iteration. Meanwhile, an experimental performance, operated by robot arm "DR-400" to provide a steady and continuous arc welding, was also conducted to verify the simulated result. By surveying the consistence of molten pool bounded by contrast shade and simulated melting contour on the surface of workpiece, the validity of model proposed to predict the thermal cracker has been successfully identified.

I. INTRODUCTION

The arc beam heating source has been widely used in precisely manufacturing field such as in drilling, welding and cutting process. Some relative restacks on this topic have been presented for past few years. Woods and Milner [5] made an experiment to predict the flow motion in the fusion zone for arc welding, and an important conclusion shows that the induced molten flow will be created out under the action of Lorentz force for higher energy density applied. Brent [1] introduced the enthalpy technique to smooth the phase change by heating the pure metal. With that, they successfully approached the stable solution and the divergent iteration at solid-liquid interface could be fully avoided. Wei [4] examined the appearance of porosities at advancing melting front in rapid solidification. In which , the tiny bubbles, squeezed into the molten pool by higher temperature of arc beam, have been captured by experimental photography and their sizes were found to grow up by absorbing additional latent heat at melting

front. If the escaping movement of bubbles fails before the chilly effect stops working, the presence of pores will lead to the thermal deficit of interfacial fracture and degrade the mechanical properties of welded samples.

Another experimental investigation on interfacial thermal conductance was undertaken by Wang [3]. Here an irregular and coarse crystal structure, observed near the phrasal interface, was identified to be arisen from the distinct interior expansion or cooling contraction and it also interprets that the overheating or quick freezing phenomena might have been experienced. In addition, a quantitative analysis of heat transfer coefficient at liquid-solid front was proposed by Viskanta [2]. In which, the jumping increase of thermal property had been achieved by analytic approach and experimental measurement. While observe the discontinuous thermal property at time-dependent solid front, exceptional heat flux rate should be dissipated or removed out in a short duration. Otherwise, it gives rise to the distortion of meting interface and the thermal crack will be resulted.

For the papers released before, most were focused on the experimental process to discuss the global behavior of phase change during the melting process , but less were subjected to predict the thermal crack of the material via the distribution of temperature gradient inside the workpiece. With the estimation of smaller Pelect number and Renold number in this study, the agitation of melting flow could be neglected and which offers a special advantage to simplify the simulated model. Through 3-D quasi-steady transformation in enthalpy method, the thermal crack inside the workpiece could be easily predicted from the unusual distribution of the isothermal contours estimated, and the welding characteristic consistent with experimental observation can be also reasonably explained.

II. ANALYTIC METHOD

A sketch of welded channel melt by moving arc system, along x direction, is illustrated in Fig. 1. In order to ensure the steady melting process simulated, a quasi- steady transformation should be made, i.e. the reference coordinate has to be imposed on the moving source where the coordinate has to be transferred from $(t, \bar{X}, \bar{Y}, \bar{Z}) \rightarrow (\tau, x, y, z)$ by chain rules. Since the smaller liquid Pelect number, less than 2, is estimated, the flow motion of molten metal and convective terms in the fusion zone can be ignored. Hence a simplified model
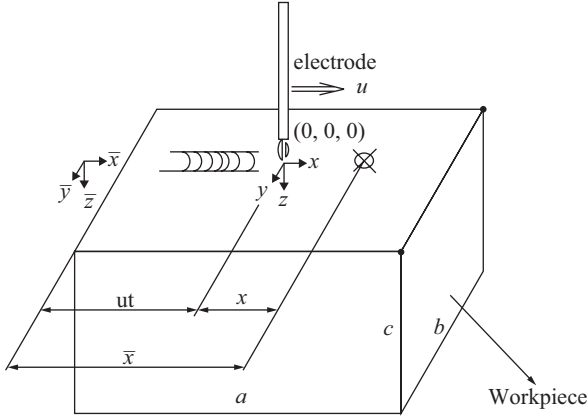
Fig. 1. The coordinates in heating unit.

with above assumptions will be proposed and represented by Eq. (1)

$$-\rho u \frac{\partial H}{\partial x} = K_i \left(\frac{\partial^2 T}{\partial x^2} + \frac{\partial^2 T}{\partial y^2} + \frac{\partial^2 T}{\partial z^2} \right) \qquad (1)$$

$$H = \begin{cases} C_s T & T < T_m - \varepsilon \\ C_s T + \dfrac{h_{sl}}{2\varepsilon}(T - T_m + \varepsilon) & T_m - \varepsilon \le T \le T_m + \varepsilon \\ C_l T + h_{sl} & T_m + \varepsilon < T \end{cases}$$

where enthalpy function H was also required to be considered to maintain the continuous property at the solid-liquid interface and small value of ε (0.01k) is assumed for the numerical modeling

Associated with the governing Eq. (1), thermal energy balance between the conduction heat and convection to surrounding are specified on boundary surfaces as given in Eqs. (2)-(7), and the moving heating source with energy flux of Gauss distribution is imposed on the electrode.

$$x = -\frac{a}{2} \qquad K_i \frac{\partial T}{\partial x} = h(T - T_\infty) \qquad (2)$$

$$x = \frac{a}{2} \qquad -K_i \frac{\partial T}{\partial x} = h(T - T_\infty) \qquad (3)$$

$$y = -\frac{b}{2} \qquad K_i \frac{\partial T}{\partial y} = h(T - T_\infty) \qquad (4)$$

$$y = \frac{b}{2} \qquad -K_i \frac{\partial T}{\partial y} = h(T - T_\infty) \qquad (5)$$

$$z = c \qquad -K_i \frac{\partial T}{\partial z} = h(T - T_\infty) \qquad (6)$$

$$z = 0 \qquad K_i \frac{\partial T}{\partial z} = q e^{-\frac{r^2}{2\sigma^2}} \qquad (7)$$

where $r = \sqrt{x^2 + y^2}$, $q = \dfrac{Q}{\pi \sigma^2}$.

III. NUMERICAL METHOD

For simplicity, working parameters should be generalized as an important dimensionless parameter, global pelect number, which has been developed and given as

$$p_e = \frac{ua}{\alpha} \qquad \alpha = \frac{K_i}{\rho C_s} \qquad (8)$$

where u is the melting velocity, a is the length of the workpiece and then α is defined as the thermal diffusivity of material.

Before the numerical analysis is in progress, governing equations in nondimensional forms should be done in advance. In this study, melting temperature, length of the workpiece and melting velocity are chosen as the characteristic values corresponding to the individual physical quantity. Variables in above questions can be normalized by dividing the individual characteristic value, and then all the symbols appearing below will be taken as the dimensionless variables. Invoking the backward difference in upwind scheme for first derivative and the central difference for second derivative terms, we can obtain, after rearrangement, the following discretization equation for governing Eq. (1):

$$\begin{aligned} AA * T(i, j, k) &= BB * T(i+1, j, k) \\ &+ CC * T(i-1, j, k) + DD * T(i, j+1, k) \\ &+ EE * T(i, j-1, k) + FF * T(i, j, k+1) \\ &+ GG * T(i, j, k-1) + T^n(i, j, k)\left(\frac{1}{\Delta t}\right) \end{aligned} \qquad (9)$$

where

$$AA = \left(\frac{u}{\Delta x} + \frac{1}{\Delta t} + \frac{6}{P_e \Delta x^2} \right) \qquad BB = \left(\frac{u}{\Delta x} + \frac{1}{P_e \Delta x^2} \right)$$

$$CC = \left(\frac{1}{P_e \Delta x^2} \right) \qquad DD = \left(\frac{1}{P_e \Delta y^2} \right)$$

$$EE = \left(\frac{1}{P_e \Delta y^2} \right) \qquad FF = \left(\frac{1}{P_e \Delta z^2} \right)$$

$$GG = \left(\frac{1}{P_e \Delta z^2} \right)$$

IV. EXPERIMENTAL PROCEDURE

To assure a better quality in the fusion zone, a experiment mechanism resorted to FATW welding electrode, "Dynasty 300 DX" positioned on the machinery robot "DR-400", was
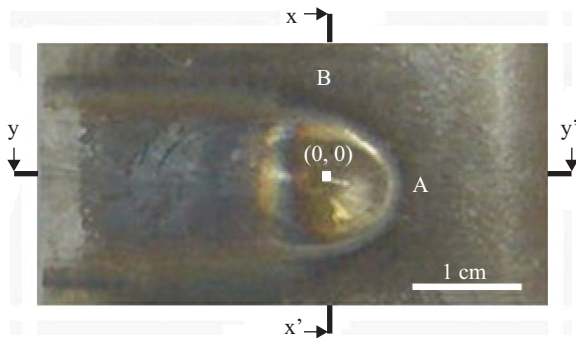
Fig. 2. The top view of heated workpiece with 1 mm/s under incident power 6.8 kw applied.
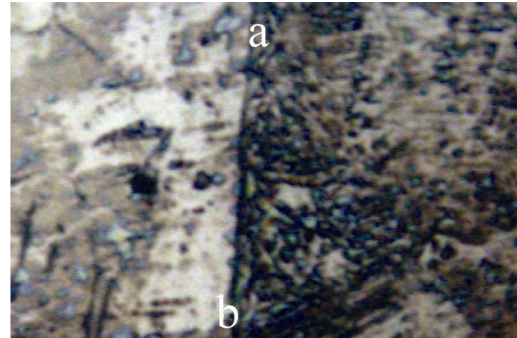

Fig. 3. The micro image at A point with a magnification of 800 x.
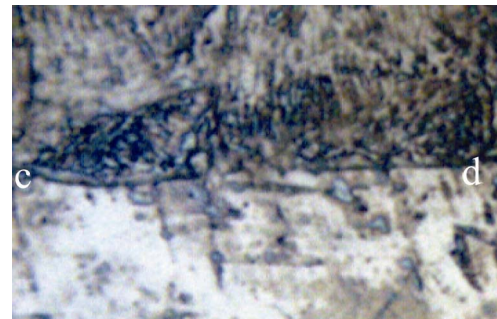

Fig. 4. The micro image at B point with a magnification of 800 x.

set up to provide a safe operation. Carbon steel 304 with dimensions 5 cm × 3 cm × 1 cm was chosen as the workpiece, which has to be grinded in advance to remove the oxidization layer on its top surface. The polishing with Al_2O_3 mixing liquid and etching step with 3% dilute HCl solution should be also involved for the post-treatment of the welded sample. According to the individual test in this experiment, the working current 160A, 180A, 200A, 220A and 240A was set respectively and then the feed speed 1.5 mm/s, 2 mm/s, 2.5 mm/s, 3 mm/s and 3.5 mm/s was regulated by turns.

V. RESULT AND DISCUSSION

1. For present model, an simulated matrix in diagonal dominance, all the coefficients A, a, b, c ,d in the discrimination equations are positive and A > a + b + c + d , can be constituted. It satisfies the convergent condition of the Gauss-Seidel's algorithm and Scarborough criterion. Hence an approximate result without over restricting the grid size will be accessed by using the finite difference in upward scheme. Moreover, available Pe value can be further extended until the unstable iteration begins to emerge as the pe value reaches 500.

2. Though the first order truncation error (ΔX, ΔY, ΔZ) is derived in upwind scheme method, the smaller step size ΔX, ΔY, ΔZ with increased grids are required to ensure the more accurate solution. In this study, grids 20 × 30, 30 × 45, 40 × 60 were selected to distribute uniformly in the calculating domain and the convergent solutions will be approached using the relaxation coefficient 0.75~1.2. Compared with individual result obtained from grids test, their maximum relative error will be found not more than 3%, and then the grids 20 × 30 has been proven to be adequate to clearly describe the molten characteristic of welded channel without losing the overall behavior.

3. Observation from the picture in Fig. 2, three distinctive shades of color reflected from the welded channel is visualized and which corresponds to important physical meaning respectively. First, the white- hot spot, located at (0, 0), specifies the location of the highest temperature in molten pool ,where the input energy is irradiated on directly. Secondly, the contrast shade of color arising from the larger temperature slope is usually predicted along the semicircle boundary of the spot. Finally, the uniform gray shade, at the immediate neighbor and rear to the hot spot, tells the surface temperature below melting point has been still kept. While scanning the surface appearance of the welded channel using the microscope with magnification of 800 x, photographs with different crystal structure could be captured around the border of the hot spot, i.e., the louts of semi-periphery passing through A, B is followed in Fig. 2.

4. Among these pictures, microscope images at points A and B showing the molten region with brighter reflection and upcoming solid metal in dark shade, separated by lines ab and cd, are displayed in Fig. 3 and Fig. 4 respectively. Thus the mentioned separating lines correlated with two phase transition indicates the location of fusion front during the melting process, which is just the position of residual crack compressed by different cooling contraction for both phase. Classified from above demonstration, the surface fracture caused by cooling contraction is believed to survive somewhere in the presence of contrast shade. Beside, the inherent defect could be confirmed experimentally near the liquid and solid interface, where exhibits the maximum temperature gradient during the melting process, i.e., the fastest cooling rate occurring in the solidification will be also predicted there in the inverse process.

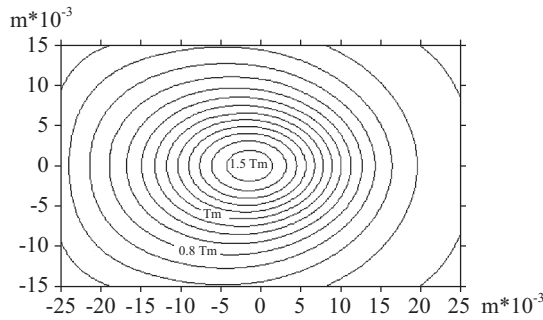5. Compared with the experimental results in Figs. 2-4 the

Fig. 5. The simulated temperature distribution of the top view with traveling speed 1 mm/s under incident power 6.8 kw applied.
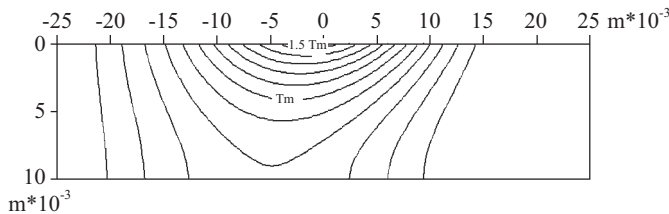

Fig. 6. The simulated temperature distribution of x-x' section view with traveling speed 1 mm/s under power 6.8 kw applied.

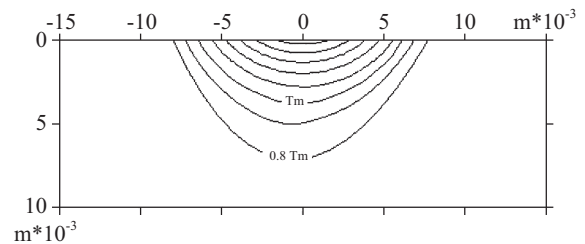**Fig. 7.** The x-x' section view of heated workpiece with traveling speed 1 mm/s under incident power 6.8 kw applid.

Fig. 8. The simulated temperature distribution of y-y' section view with traveling speed 1 mm/s under incident power 6.8 kw applied.

preliminary contribution of the proposed model can be confirmed by inspecting the simulated oval-shaped molten pool in Fig. 5, bounded with melting isothermal contour T_m, and which is agreement with the molten pools measured in Fig. 2. In addition, the distribution of isothermal contours is highly concentrated, along the contour T_m, at the semi-periphery ahead of the hot spot, where the thermal fracture in maximum temperature gradient will be created out as the surface chilling of working sample is in progress. Referred to above prediction, the simulated location of the residual crack has been identified to be close to the situation indicated from the experimental measurement. On the other hand, the temperature distribution resided at x-x' cross section, as shown in Fig. 6, was also selected to examine the interior crack of workpiece. In which, the isothermal contour in high dense distribution is primarily riveted on the front of the heating source. Here the serious crack will be expected here after the cooling process, and it will become worse provided that faster traveling speed of electrode is in use. Based on above statement, most of the incident energy will be believed to preheat the upcoming material, along the travel direction, instead of penetrating into the workpiece and the prediction made above can also clearly interprets the facts that the exceptional surface deposition of isocontours, ahead of the electrode tip, will induced the non-equilibrium of heat transfer at contour T_m, and which easily leads to the cooling crack at working surface. That is also agreement with the results obtained from Fig. 2.

6. To further correct the validity of proposed model, the inspection of temperature distribution at y-y' section was required and the outcomes attained from experiment and numerical simulation was then depicted in Fig. 7 and Fig. 8 respectively. While survey the picture photographed in Fig. 7, a produced semicircle fusion zone, molten width is nearly triple as long as the scale of depth has been carried out and which could be identified by the numerical result outlined in Fig. 8 where the molten region surrounded by melting contour T_m, depth 3.5 mm and width 12 mm, is indicated. From above demonstration, more heat flux transferred to enhance the width of the pool, due to the denser temperature gradient in radial direction, rather than conducted downwards to penetrate into the depth might be further confirmed by visualizing the isothermal contours of fusion zone in Fig. 8. So the wider opening of the molten pool emerging in simulated result seems to be not surprised, and which is also compatible with the cross section view shown in Fig. 7. Furthermore, the inner breakage at the melting surface could be also inferred from Fig. 6 and Fig. 8, where the difference of temperature gradient along the radial direction will approach the maximum value. Therefore the crack with outward extension from the melting interface will be also expected.

VI. CONCLUSION

Classify from above discussion, several important conclusions might be made as follows:

(1) Diagonal dominance by invoking the finite difference in upwind scheme satisfies the convergent condition of Gauss-Seidel iteration, and the restriction of relaxation value, 0.75~1.2, will accelerate the convergent procedure.

(2) A divergent iteration during computational process could be avoided by proposing the enthalpy method in this study, where the continuous property along the solid-liquid interface will be ensured.

(3) Since the aspects of melting pool with ratio of meting width to depth, 2.5~3, are always followed, the prediction of more energy estimated to make the fusion zone wider, instead of penetrating into the molten base, seems to be reasonable.

(4) The exposure of interior fracture, arising from the residual thermal stress, is primarily determined by the distribution of the isothermal contours and which usually appears at the melting surface of molten zone, where more heat flux in higher temperature gradient will be released rapidly during the unstable chilling process.

(5) The serious cracking deficit caused by cooling contraction will be survived at the front of heating source, especially under the higher traveling speed applied.

NOMENCLATURE

C_p the thermal conductivity specific heat in both phases [$Jkg^{-1}K^{-1}$]

H C_pT enthalpy function [$Wm^{-2}K^{-1}$]

T temperature [K]

T_m melting temperature of the workpiece [K]

U feed velocity [ms^{-1}]

Q incident power [kW]

K_i thermal conductivity, k_l or k_s [$Wm^{-1}K^{-1}$]

$\bar{X}$ the absolute reference coordinate in the direction of feed velocity

$\bar{Y}$ the absolute reference in transversal direction

$\bar{Z}$ the vertical coordinate at absolutely reference

a length of workplace [m]

b width of workplace [m]

c hight of workplace [m]

c_l thermal specific heat in in liquid phase [$Jkg^{-1}K^{-1}$]

c_s thermal specific heat in in solid phase [$Jkg^{-1}K^{-1}$]

h thermal convective coefficient [W/m^2K]

q incident energy flux, $Q/\pi\sigma^2$ [Wm^{-2}]

r dimensional radial coordinate [m]

x the relative coordinate in the direction of feed velocity

y the relative coordinate in transversal direction

z the relative coordinate in vertical direction

ρ density of workpiece [kg/m^3]

α thermal diffusivity in both phases [m^2/s]

σ energy distribution radius [m]

Δt time step [s]

Δx space discrization size in x direction [m]

Δv space discrization size in y direction [m]

Δz space discrization size in z direction [m]

REFERENCES

1. Brent, A. D., Voller, V. R., and Reid, K. J., "Enthaply-Porosity technique for modeling convection-diffusion phase change," *Numerical Heat Transfer*, Vol. 13, pp. 297-318 (1998).

2. Viskanta, R., "Heat transfer during melting and solidification of metal," *ASME Journal of Heat Transfer*, Vol. 110, pp. 1205-1219 (1988).

3. Wang, G.-X. and Matthys, E. F., "Experimental investigation of interfacial thermal conductance for molten metal solidification," *ASME Journal of Heat Transfer*, Vol. 18, pp. 157-163 (1996).

4. Wei, P. S., "Shape of a pore trapped in solid solidification," *International Journal of Heat and Mass Transfer*, Vol. 43, pp. 263-280 (2000).

5. Woods, R. A. and Milner, D. R., "Motion in the weld pool in arc welding," *Welding Journal*, Vol. 50, pp. 163-173 (1971).